Aerodynamic and Radiative Controls on the Snow Surface Temperature

J. W. POMEROY

Centre for Hydrology, University of Saskatchewan, Saskatoon, Saskatchewan, Canada

R. L. H. ESSERY

School of Geosciences, University of Edinburgh, Edinburgh, United Kingdom

W. D. HELGASON

Civil and Geological Engineering, University of Saskatchewan, Saskatoon, Saskatchewan, Canada

(Manuscript received 18 November 2015, in final form 26 April 2016)

ABSTRACT

The snow surface temperature (SST) is essential for estimating longwave radiation fluxes from snow. SST can be diagnosed using finescale multilayer snow physics models that track changes in snow properties and internal energy; however, these models are heavily parameterized, have high predictive uncertainty, and require continuous simulation to estimate prognostic state variables. Here, a relatively simple model to estimate SST that is not reliant on prognostic state variables is proposed. The model assumes that the snow surface is poorly connected thermally to the underlying snowpack and largely transparent for most of the shortwave radiation spectrum, such that a snow surface energy balance among only sensible heat, latent heat, longwave radiation, and near-infrared radiation is possible and is called the radiative psychrometric model (RPM). The RPM SST is sensitive to air temperature, humidity, ventilation, and longwave irradiance and is secondarily affected by absorption of near-infrared radiation at the snow surface that was higher where atmospheric deposition of particulates was more likely to be higher. The model was implemented with neutral stability, an implicit windless exchange coefficient, and constant shortwave absorption factors and aerodynamic roughness lengths. It was evaluated against radiative SST measurements from the Canadian Prairies and Rocky Mountains, French Alps, and Bolivian Andes. With optimized and global shortwave absorption and aerodynamic roughness length parameters, the model is shown to accurately predict SST under a wide range of conditions, providing superior predictions when compared to air temperature, dewpoint, or ice bulb calculation approaches.

1. Introduction

The snow surface temperature (SST) is an important variable in energy balance calculations of snowpack energetics and as a lower boundary condition for the atmosphere over snow-covered surfaces (King et al. 2008). The SST is defined here as the temperature responsible for longwave exitance and is not the temperature of the uppermost few centimeters of the snowpack. It forms the basis for calculations of longwave emission from the snow cover and a lower reference condition for calculations of sensible and latent heat flux (Kondo and Yamazaki 1990; Marks and Dozier 1992; Fierz et al. 2003). These calculations govern the coupled energy and mass budget equations that determine snow dynamics, particularly the energy state of snow, surface sublimation, and snowmelt. Various methods exist to estimate SST, including the assumption that it is at 0°C when melting occurs and is otherwise related to air temperature when net radiation is positive (Jordan 1991; Marsh and Pomeroy 1996), modified force–restore techniques (e.g., Luce and Tarboton 2010), heat conduction equations (e.g., Tarboton and Luce 1996; Raj Singh and Yew Gan 2005), dewpoint methods (Andreas 1986; Raleigh et al. 2013), and methods that employ the coupled mass and energy balance equations including radiation to snow (Kondo and Yamazaki 1990; Jordan 1991; Lehning et al. 2002; Ellis

Corresponding author address: John Pomeroy, Centre for Hydrology, University of Saskatchewan, 117 Science Place, Saskatoon, SK S7N 5C8, Canada.
E-mail: john.pomeroy@usask.ca

DOI: 10.1175/JHM-D-15-0226.1

et al. 2010). Many land surface schemes (LSSs) for atmospheric models include explicit SST calculations; these are usually coupled energy and mass balance calculations for an infinitesimal "skin" layer of snow [e.g., Canadian Land Surface Scheme (CLASS; Verseghy 1991; Verseghy et al. 1993), Community Land Model (CLM; Oleson et al. 2008), and Joint UK Land Environment Simulator (JULES; Best et al. 2011)], though a version of the Interactions between Soil, Biosphere, and Atmosphere (ISBA) model uses the force–restore method (Douville et al. 1995). Evaluation of LSS performance over snow has suggested that most LSSs become too cold over the winter, and this could be partly due to an overestimation of longwave energy loss from snowpacks in some of these models (Slater et al. 2001). Energy balance snow models used for hydrology and snow dynamics vary from single-layer models such as the energy-budget snowmelt model (EBSM; Gray and Landine 1988) to more physically detailed layered models such as SNOBAL (Marks et al. 1999, 2008), SNTHERM (Jordan 1991), Crocus (Brun et al. 1989, 1992; Vionnet et al. 2012), and SNOWPACK (Bartelt and Lehning 2002). Marks et al. (2008) have shown that the performance of physically based layered snowmelt models is very sensitive to how the upper model snow layers are parameterized. A recent snow model intercomparison study found that many of the models had significant discrepancies in their longwave exitance when compared to observations (Rutter et al. 2009).

What is not always appreciated in process or modeling studies of SST is the strong difference between the temperature at the snow surface and the temperature just below or near the snow surface. A recent study (Helgason and Pomeroy 2012b) including detailed fine-wire thermocouple measurements of temperatures just below the snow surface (0–10 cm) found that they were strongly related to the 1.5-m air temperature because of convection through porous media; in contrast, radiometrically measured surface temperatures were up to 4°C colder than the snow just below. This is consistent with microwave observations of wet snow under freezing snow surfaces (Koh and Jordan 1995) and the rapid change in SST upon exposure in a snowpit wall (Schirmer and Jamieson 2014). It is therefore important to define the snow surface temperature as that occurring on the upper boundary of the snowpack, the boundary that is responsible for longwave exitance. Because longwave radiation is not transmitted through snow or water and has a very low reflectance (Dozier and Warren 1982), this boundary is likely to be exceedingly thin and will lay above the physical layers that can be measured with fine-wire thermocouple thermometry.

The wide variety of methods and apparent deficiencies in land surface scheme and snow model estimates of longwave exitance suggest a need to more fully understand the major energy and mass fluxes that control the SST and how these might be reliably calculated outside of full mass and energy balance models. Some methods focus on the radiometric cooling of the snowpack (Marsh and Pomeroy 1996), some on conduction from the snowpack (Luce and Tarboton 2010), while others focus on the aerodynamic considerations (Andreas 1986). It would be advantageous for calculating SST if methods could avoid relying on uncertain prognostic state variables such as the internal energy of the snowpack or the albedo of the snowpack. This avoids accumulation of biases in estimating snow surface and internal energy state that are a large source of error in snow models (Essery et al. 2013).

The purpose of this paper is to document observations of SST in a wide variety of environments and to attempt to relate these observations in a tractable to the main driving aerodynamic and radiative energy fluxes via a simple predictive model with minimal driving variable and parameter requirements. Parameter uncertainty and optimality are examined to derive a robust predictive model of SST. By doing so, the relative importance of aerodynamic and radiative transfer in controlling the SST under various environmental conditions can be diagnosed and the applicability of the model for estimating SST can evaluated for global applications.

2. Theory

The longwave exitance $LW_{\uparrow}$ from a snow surface can be found using the assumption that it is a near blackbody from the Stefan–Boltzmann formulation,

$$LW_{\uparrow} = (1 - \varepsilon)LW_{\downarrow} + \varepsilon\sigma T_s^4, \quad (1)$$

where ε is the emissivity in the thermal infrared range (wavelength λ from 8 to 12 μm), $LW_{\downarrow}$ is the incoming longwave radiation to the surface, $\sigma = 5.67 \times 10^{-8}$ W m^{-2} K^{-4} is the Stefan–Boltzmann constant, and T_s is the surface temperature of the snowpack (i.e., SST) in kelvins. Dozier and Warren (1982) and Marks and Dozier (1992) showed that ε varies from 0.98 to 0.99 for snow, depending on viewing angle. Hori et al. (2006) found both an angular and a grain-size dependency on emissivity, with values above 0.98 for fine-, medium-, and most coarse-grained snow, with exceptional values from 0.90 to 0.98 for some sun crust snow where specular reflection of thermal infrared radiation was observed. In practice, many calculations (e.g., Best et al. 2011) assume that $\varepsilon = 1$. The critical variable to estimate in Eq. (1) is the

SST (i.e., T_s), which is further defined here as the longwave radiant temperature of snow to distinguish it from the temperatures of subsurface layers that may not correspond to the thermal radiating surface (Helgason and Pomeroy 2012b).

Many procedures to estimate SST (Armstrong and Brun 2008) employ a form of the energy balance, where the SST is found as the result of an iterative or linearized solution to the energy equation for snow:

$$\mathrm{SW}^* + \mathrm{LW}^*(T_s) + \mathrm{LE}(T_s) + H(T_s) + G = M + \frac{dU}{dt}, \tag{2}$$

where SW* is net shortwave radiation, LW* is net longwave radiation, LE is the latent heat flux due to sublimation, H is the sensible heat flux to the snow, G is the ground heat flux, M is the latent heat flux due to melting, U is internal energy state of the snow, and t is time. The net longwave, sensible, and latent heat flux terms are a function of the SST in regard to their surface reference conditions. The disposition of energy between M and internal energy change is also controlled by snow temperatures, including the SST. However, solving for the SST from an energy budget such as Eq. (2) presumes that 1) the SST is well-coupled to that of the underlying snowpack and 2) all snowpack mass and energy exchanges with the atmosphere occur exactly at the surface. Some procedures try to compensate for this by calculating the energy state of multiple layers in a snowpack (e.g., Jordan 1991) or separating a surface layer calculation from the bulk snowpack temperature calculation using a heat conduction term (e.g., Verseghy et al. 1993). Kondo and Yamazaki (1990) remove the shortwave component from the energy balance of the surface layer, assuming complete reflection and transmission of shortwave radiation through the surface and absorption in interior snowpack layers. These compensations still need to estimate a fairly comprehensive set of energy exchange calculations at the surface, as well as the snow thermal conductivity, ground heat flux, and an internal snowpack temperature gradient. Cumulative errors in estimating internal snow energy state can cause large errors in the radiative balance and turbulent exchanges with snow (Pomeroy et al. 1998; Helgason and Pomeroy 2012b).

A photograph taken of an upper layer of a natural late-winter snowpack in Yukon, Canada, shows a ''skin'' layer at the surface that appears to be not well structurally connected to the rest of the snowpack (Fig. 1). Individual snow crystals at the top of the snowpack are well exposed to the atmosphere and tenuously connected to the rest of the snowpack by slender bonds. This

FIG. 1. A snowpack surface cross-sectional photograph taken in April 2003 in Wolf Creek Research Basin, Yukon, Canada. The cold snowpack has poorly bonded surface crystals and displays light penetration indicative of its porous medium nature.

is a typical condition for snow; snow surfaces are often composed of a persistent surface hoar with a very sparse bond structure connecting these crystals to the ice matrix below (Hachikubo and Akitaya 1997; Stössel et al. 2010). In this layer the tenuous bonds that connect the top surface crystals to the rest of the snowpack will conduct very little heat because of their low thermal conductivity and will have a very small heat capacity, as shown by the measurements of Helgason and Pomeroy (2012b). This structure suggests that the surface may be poorly coupled by heat conduction with the rest of the snowpack, and therefore the usefulness of Eq. (2) in estimating T_s needs to be reassessed. As liquid water and ice are exceedingly poor transmitters of thermal infrared radiation, it can be presumed with confidence that only the outer surface layer of the upper layer of crystals of this snowpack is active in emitting longwave radiation. Further, one may assume that the outer surface layer reflects or transmits most of the incident visible shortwave radiation (Kondo and Yamazaki 1990), but absorbs some of the near-infrared (NIR) shortwave radiation, depending on grain size (Wiscombe and Warren 1980), mineral dust, biological materials, and black organic carbon (Dang et al. 2015). This system is analogous to an aspirated ice bulb with longwave and NIR radiative inputs. From these considerations, a greatly simplified model of the energy balance in relation to the snow surface temperature can be proposed as

$$\mathrm{NIR}^* + \mathrm{LW}^*(T_s) + \mathrm{LE}(T_s) + H(T_s) = 0. \tag{3}$$

Here it is understood that the NIR* term is not normally measured and that it can be found as a function of net

shortwave irradiance at the snow surface. This radiative psychrometric model (RPM) of SST has certain operational advantages over other methods in that it 1) does not require information on the energy state of the snowpack or substrate and 2) requires only standard atmospheric information (wind speed, temperature, and humidity) and incoming radiation. The terms in the RPM are parameterized as

$$f_{\text{abs}}\text{SW}_{\downarrow} + \varepsilon(\text{LW}_{\downarrow} - \sigma T_s^4) = \frac{\rho}{r_a}\{c_p(T_a - T_s) + L[Q_a - Q_{\text{sat}}(T_s, P_s)]\}, \quad (4)$$

where f_{abs} is a surface shortwave radiation ($\text{SW}_{\downarrow}$) absorption factor to help estimate NIR* from incoming shortwave radiation measurement (if 1 then all radiation is absorbed, if 0 then no radiation is absorbed); ε is the emissivity of snow, taken as 0.985; ρ is the air density (kg m^{-3}); r_a is the aerodynamic resistance (s m^{-1}); $c_p = 1005\,\text{J kg}^{-1}\,\text{K}^{-1}$ is the specific heat capacity of air; $L = 2.835 \times 10^6\,\text{J kg}^{-1}$ is the latent heat of sublimation; Q_a is the specific humidity of the air; and T_a is the air temperature. The term $Q_{\text{sat}}(T_s, P_s)$ is the saturation specific humidity at snow surface temperature T_s and surface air pressure P_s, which can be approximated by the Buck (1981) formula,

$$Q_{\text{sat}} = \frac{3.8}{P_s}\exp\left(\frac{22.452T}{272.55 + T}\right), \quad (5)$$

for temperature in degrees Celsius and pressure in hectopascals. For application to the snow surface, $T = T_s$. Neglecting corrections for atmospheric stability near to the surface (Andreas 1986), the aerodynamic resistance can be found as

$$r_a = \frac{1}{uk^2}\ln\left(\frac{z_T}{z_0}\right)\ln\left(\frac{z_u}{z_0}\right), \quad (6)$$

where $k = 0.4$ is the von Kármán constant, u is the wind speed (m s^{-1}) at height z_u (m), z_T is the measurement height of the air temperature T_a, and z_0 is the aerodynamic roughness length for snow (m). For simplicity, aerodynamic exchange in RPM does not consider stability corrections, and anemometer stall speeds (assumed $0.1\,\text{m s}^{-1}$) are the lowest wind speeds used to drive Eq. (6). The lack of stability corrections is supported by the uncertainty in stability corrections found from careful field tests in mountains (Stössel et al. 2010; Martin and Lejeune 1998; Helgason and Pomeroy 2012a) and level sites (Helgason and Pomeroy 2012b).

The left-hand side of Eq. (4) is radiative and the right-hand side is aerodynamic. Under conditions of low ventilation (high r_a) it can be presumed that the radiative terms will dominate calculation of the snow surface temperature, and under high ventilation (low r_a) aerodynamic terms will become more important. The relative contribution of radiative and aerodynamic terms can be described by apportioning the SST between a radiative equilibrium temperature $T_{r_{\text{eq}}}$ and an aerodynamic equilibrium temperature $T_{a_{\text{eq}}}$. The radiative equilibrium temperature can be found using the Stefan–Boltzmann equation and the assumption that the SST is determined completely by radiation balance, giving

$$T_{r_{\text{eq}}} = \left(\frac{f_{\text{abs}}\text{SW}_{\downarrow} + \varepsilon\text{LW}_{\downarrow}}{\varepsilon\sigma}\right)^{1/4}. \quad (7)$$

The aerodynamic equilibrium temperature for full ventilation (the ice bulb temperature) can be found for the condition $r_a = 0$ as

$$T_{a_{\text{eq}}} = T_a + \frac{L}{c_p}[Q_a - Q_{\text{sat}}(T_{a_{\text{eq}}}, P_s)]. \quad (8)$$

Note that this is an implicit equation that requires an iterative solution for $T_{a_{\text{eq}}}$. Apportionment of the SST between radiative and aerodynamic equilibria is governed by the degree of ventilation, such that

$$T_s = (1 - f_v)T_{r_{\text{eq}}} + f_v T_{a_{\text{eq}}}, \quad (9)$$

and f_v is a ventilation factor varying from 0 for an aerodynamically decoupled surface ($r_a = \infty$) to 1 for a perfectly ventilated surface ($r_a = 0$). Rearranging Eq. (9) to solve for f_v in terms of aerodynamic equilibrium, radiative equilibrium, and SST gives

$$f_v = \frac{T_s - T_{r_{\text{eq}}}}{T_{a_{\text{eq}}} - T_{r_{\text{eq}}}}, \quad (10)$$

which shows that as the SST approaches radiative equilibrium and/or the difference between the aerodynamic and radiative equilibrium temperatures increases, then f_v approaches zero.

The RPM requires knowledge of air temperature, humidity, wind speed, incoming longwave and shortwave radiation, aerodynamic roughness, and atmospheric pressure (which can be measured or found from site elevation). Its parameters are snow aerodynamic roughness length and shortwave absorption factor. Aerodynamic roughness can be measured or estimated from published values. Estimation of the shortwave absorption factor at the surface requires information on the spectral distribution of shortwave radiation, the spectral albedo of the snow surface, angular reflectance,

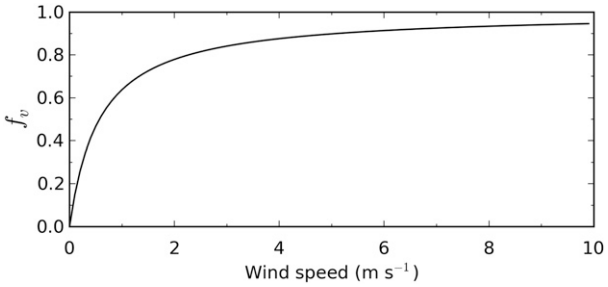

FIG. 2. Sensitivity of the ventilation factor (i. e., f_v) to wind speed for air temperature of −10°C, relative humidity of 80%, no incoming shortwave radiation, incoming longwave radiation of 250 W m^{-2}, and aerodynamic roughness length of 3×10^{-3} m. Reference height for atmospheric variables is 2 m above the snow surface.

and the extinction of NIR in snow. All of these factors vary in complex ways: the spectral distribution of radiation with atmospheric conditions and multiple reflections by vegetation and terrain; the spectral albedo of snow with surface grain size, contaminants, and liquid water content; and radiation extinction with snow structure and contamination (Pomeroy and Brun 2001). It is possible to estimate snow radiative absorption using the calculations described by Warren and Wiscombe (1980) with recent adjustments for contaminants (Dang et al. 2015), but such estimates will depend on uncertain assumptions of surface layer thickness, dust, black carbon or organic matter contamination, grain size, wetness, and site-specific spectral irradiance. This factor is expected to be small because NIR is less than half of shortwave radiation and not all NIR is extinguished at the snow surface. As such, it should be less than (1 − albedo) and so should be less than 0.1 for fresh, clean snow and less than 0.3 for dirty, wet snow.

3. Sensitivity analysis

The RPM was investigated initially with a sensitivity analysis of its driving variables using fixed parameters in order to demonstrate how wind speed influences the ventilation factor and how temperature, humidity, wind speed, and radiation influence the snow surface temperature. Figure 2 shows that the ventilation factor increases initially rapidly from 0 as wind speed increases and approaches 1 asymptotically as wind speeds become high. Wind speed, temperature, and humidity for this example are from a reference height of 2 m above the snow surface, and relative humidity is with respect to ice. Example conditions are relative humidity = 80%, incoming longwave radiation = 250 W m^{-2}, and wind speed = 2 m s^{-1}. The rapid rate of change in f_v for low wind speeds shows that only a moderate degree of ventilation is required for aerodynamic equilibrium conditions to dominate SST; the effect of low wind speed is to decouple the surface temperature from aerodynamic effects and so it becomes dominated by radiation. Figure 3 shows T_s, $T_{a_{eq}}$, and $T_{r_{eq}}$ similarly estimated using the RPM as a function of wind speed, relative humidity, and incoming longwave radiation. Figure 3a shows the strong influence of air temperature on the aerodynamic equilibrium temperature but not on the radiative equilibrium. There is a nexus where $T_{r_{eq}}$, T_s, and $T_{a_{eq}}$ are equal: for air temperatures below that of the nexus, T_s is elevated above the air temperature, and for air temperatures greater than the nexus, T_s is depressed relative to the air temperature reflecting contributions from both aerodynamic and radiative components of the energy balance in controlling the SST. The nexus point and relative T_s elevation and depression are specific to the example conditions. As the relative humidity and wind speed increase, T_s and $T_{a_{eq}}$ rise toward T_a (Figs. 3b,d) and, consistent with Fig. 2, as wind speed increases, T_s moves closer to the aerodynamic equilibrium and farther from the radiative equilibrium. As irradiance increases (Fig. 3c), T_s and $T_{r_{eq}}$ increase until they surpass the constant aerodynamic equilibrium temperature, crossing at a nexus where $T_{r_{eq}}$, T_s, and $T_{a_{eq}}$ are equal. For low irradiance (below the nexus), $T_{a_{eq}}$ is greater than $T_{r_{eq}}$, and increasing the wind speed causes T_s to increase. For high irradiance (above the nexus), $T_{r_{eq}}$ is greater than $T_{a_{eq}}$, and increasing the wind speed causes T_s to decrease. The sensitivity analysis shows that solutions that consider both radiative and aerodynamic factors are necessary to calculate the snow surface temperature for a wide range of environmental conditions.

4. Observations

Observations of driving meteorology and snow surface temperatures to parameterize and test the RPM were taken at mountain pasture, lake, glacier, prairie pasture, and agricultural field sites in North and South America and obtained from data carefully collected by Météo-France in a large forest clearing mountain site in Europe. Data collection at the Americas sites was during periods of frequent site visits, which included frequent radiometer checking and cleaning. Kipp and Zonen (KZ) net radiometers (CNR1) were heated to reduce frost and snow accumulation. Data collection at the Météo-France site involved hourly cleaning of radiometers to ensure high-quality measurements over a long time period. All sites except for the French site had uniform, level fetches of at least 100 m with short or

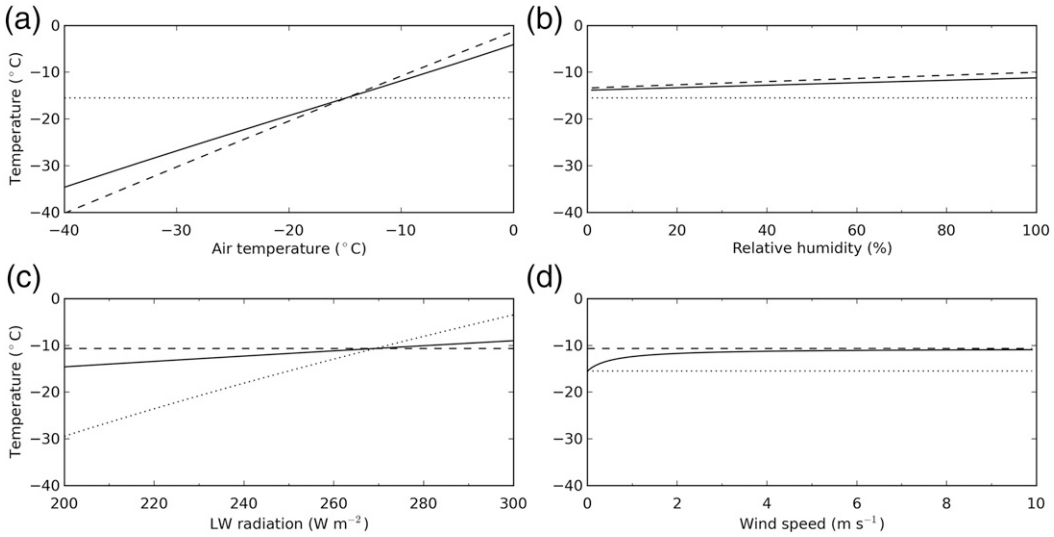

FIG. 3. Sensitivity of simulated SST (solid line), aerodynamic equilibrium temperature (dashed line), and radiative equilibrium temperature (dotted line) to variations in (a) air temperature, (b) relative humidity, (c) incoming longwave radiation, and (d) wind speed for an aerodynamic roughness length of 3×10^{-3} m and no incoming shortwave radiation. Reference heights for atmospheric variables are 2 m above the snow surface. As each variable is changed, the others are kept fixed at an air temperature of −10°C, relative humidity of 80%, incoming longwave radiation of 250 W m^{-2}, and wind speed of 2 m s^{-1}.

nonexistent vegetation. Site locations and photographs are shown in Fig. 4 and site descriptions follow. Table 1 lists instrumentation used to measure snow surface temperature and the driving meteorological variables.

a. *Pomeroy Acreage*

The Pomeroy Acreage site is located in Saskatchewan, Canada (52°02′N, 106°38′W; 508 m MSL). Measurements were taken every 15 min over an undulating, snow-covered prairie grassland with greater than 100 m of open fetch in central Saskatchewan, Canada, 6 km south of the city of Saskatoon, from 15 February to 19 March 2004. The region sustains a subhumid continental climate with cold, dry winters. The site was snow covered with at least 25 cm snow depth throughout the experiment, but a small amount of grass was exposed above the snow surface.

b. *Kernen Farm*

The Kernen Farm site is located in Saskatchewan, Canada (52.09°N, 106.31°W; 512 m MSL). Measurements were taken every 15 min as part of a study published by Helgason and Pomeroy (2012b) over a level cultivated fallow field with greater than 100 m of fetch, 2.5 km east of the city of Saskatoon, from 23 January to 2 March 2007. Climate is similar to the Pomeroy Acreage. The site was snow covered throughout the experiment with a depth of approximately 42 cm.

c. *Mud Lake*

The Mud Lake site is located in Alberta, Canada (50°47′N, 115°18′W; 1896 m MSL). Measurements were taken every 30 min on a frozen lake surface with greater than 100 m of fetch in the Spray Valley, Canadian Rockies, from 24 to 30 January 2006. This is a cold continental site with deep, even snow covering the lake with at least 80 cm depth. The site experiences significant shading from surrounding mountains in January.

d. *Zongo Glacier*

The Zongo Glacier site is located in Bolivia (16°15′S, 68°10′W; 5150 m MSL). Measurements were taken every 30 min from 8 to 16 August 2004 as part of a joint France–Canada study at a site with more than 100 m of fetch described by Sicart et al. (2005) on a flat, snow-covered lower lobe of the Zongo Glacier, Huayna Potosi Massif, Cordillera Real, Bolivia. Climate is typical of tropical glaciers, and the austral winter was cool with occasional snowfall. The surface was primarily covered with a shallow snow cover, but glacier ice patches were exposed during the measurement period.

e. *Col de Porte*

The Col de Porte site is located in France (45.30°N, 5.77°E; 1325 m MSL). Measurements as part of a study published by Morin et al. (2012) were taken every 60 min

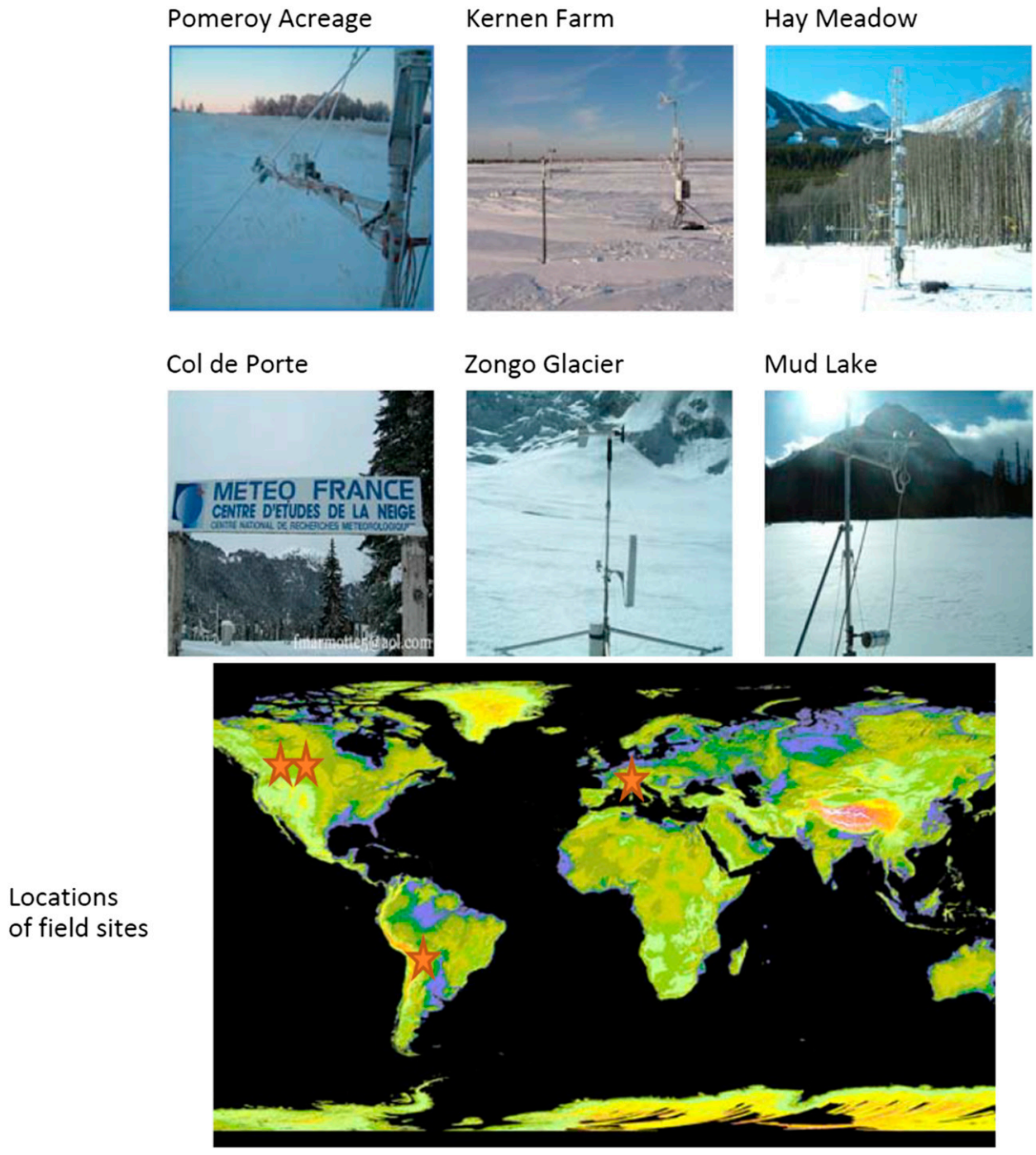

FIG. 4. Location of field sites and site photographs.

by Météo-France over a mown grass surface in a forest clearing in a mountain pass, Chartreuse mountain range, French Alps from 1993 to 2011. The forest edge on three sides was initially 25–50 m from the instruments, and a large building was 50 m away on the fourth side. Forest clearing after 1999 left forest on two sides and the large building on the other. Shading by trees and mountains occurs at this site in winter. The climate is temperate humid continental with substantial snowfall and mild winter temperatures. Snow depth exceeds 50 cm for much of the winter, and shallow snow periods were excluded from our analysis.

TABLE 1. Instrumentation used at various sites.

	Snow surface temperature	Wind speed	Temperature and humidity	Shortwave and longwave radiation
Pomeroy Acreage, Canada	Exergen IRt/c, KZ CNR1	Met One 014A 3-cup	Vaisala HMP45	KZ CNR1
Kernen Farm, Canada	KZ CNR1	Met One 014A 3-cup	Vaisala HMP45	KZ CNR1
Mud Lake, Canada	KZ CNR1	Campbell Scientific CSAT3 sonic	Vaisala HMP45	KZ CNR1
Zongo Glacier, Bolivia	KZ CNR1	R.M. Young wind monitor	Vaisala HMP45	KZ CNR1
Col de Porte, France	Exergen IRt/c, KZ CG4	Laumouier	Vaisala HMP35/45	Epply PIR/KZ CG4, KZ CM7/14
Hay Meadow, Canada	KZ CNR1	Met One Sonic	Vaisala HMP45	KZ CNR1

f. Hay Meadow

The Hay Meadow site is located at Marmot Creek, Alberta, Canada (50°56′N, 115°08′W; 1436 m MSL). Measurements as part of a study by Helgason and Pomeroy (2005, 2012a) were taken every 30 min from a large, gently sloping, grass-covered clearing with at least 60 m fetch in a mixed-wood forest in Marmot Creek Research Basin, Kananaskis Valley, Canadian Rocky Mountains, from 13 February to 5 March 2005. The site was snow covered throughout the experiment with a depth greater than 15 cm, but a small amount of sparse grass was exposed above the snowpack.

5. Analysis

The RPM was run with the time step available from the dataset (15–60 min) over the six sites, five of them with observations available for one snow season and one site for 18 seasons, depending on data availability. To investigate sensitivity to model parameters, the model was run 1681 times for each of the sites with 41 values of the surface shortwave radiation absorption factor in linear increments from 0 to 1 and 41 values of the aerodynamic roughness length in logarithmic increments from 10^{-4} to 1 m. A 35-day calibration and demonstration season (January 2006) was chosen from the large Col de Porte dataset. Figure 5 shows contour plots of root-mean-square (RMS) differences between simulated and measured surface temperatures from these runs. For each site, a unique parameter combination that minimizes the root-mean-square error (RMSE) without equifinality was found; these parameter values, along with minimum RMSEs and corresponding average errors (bias) in surface temperature, are given in Table 2. The optimized shortwave absorption factor was small (<15%) for all sites, and from very small (<5%) to zero at two sites. The smaller absorption factors occurred at the higher-latitude midwinter sites in Canada where there were no local sources of dust or organic material (Hay Meadow sometimes had some sparse exposed grass above and on the snow and was near a gravel road, which was a source of dust), suggesting that NIR absorption effects on SST are primarily important for conditions where dust, organic material, and black carbon deposition may occur. Dust deposition is more common on snow in temperate and tropical mountain environments where there are nearby geological sources. The optimized roughness length was quite variable between sites, varying from 0.001 m for Mud Lake to 0.063 m for Col de Porte. The optimal roughness length for the four flat, long fetch sites in the Canadian Prairies and mountains was small, averaging 0.004 m, while higher roughness lengths on the Zongo Glacier (0.032 m) and Col de Porte (0.063 m) may reflect local boundary layer characteristics on a rough glacier and near a forest edge, respectively.

Figure 6 shows RPM simulations and observations of SST at single seasons for the six sites with the optimal parameters (Table 2) for each site. The figure illustrates the generally good fit (Table 2) of the optimized RPM to observations for a wide range of environments (from prairies to mountains to glaciers) and SST (from 0° to −40°C). The same model runs can be used to examine the behavior of the ventilation factor at the various sites (Fig. 7). The prairie sites were usually well ventilated with high f_v, except for periods when strong inversions formed under relatively calm winds—these were often at night, but substantial multiday, well-ventilated periods with high f_v were common both day and night. The nonglaciated mountain sites in Canada, both valley bottom sites, showed lower overall ventilation factors than in the prairies and stronger diurnal fluctuations consisting of high f_v during the day and low values at night. Valley bottom inversions are common after sunset in this environment and so likely explain this behavior. The Col de Porte site is partly surrounded by forest, and its highly variable but generally low f_v is likely associated with its variable fetch and forest and complex terrain influence on wind flow. The Zongo Glacier site experienced consistently high ventilation factors that are due to its drainage winds rather than

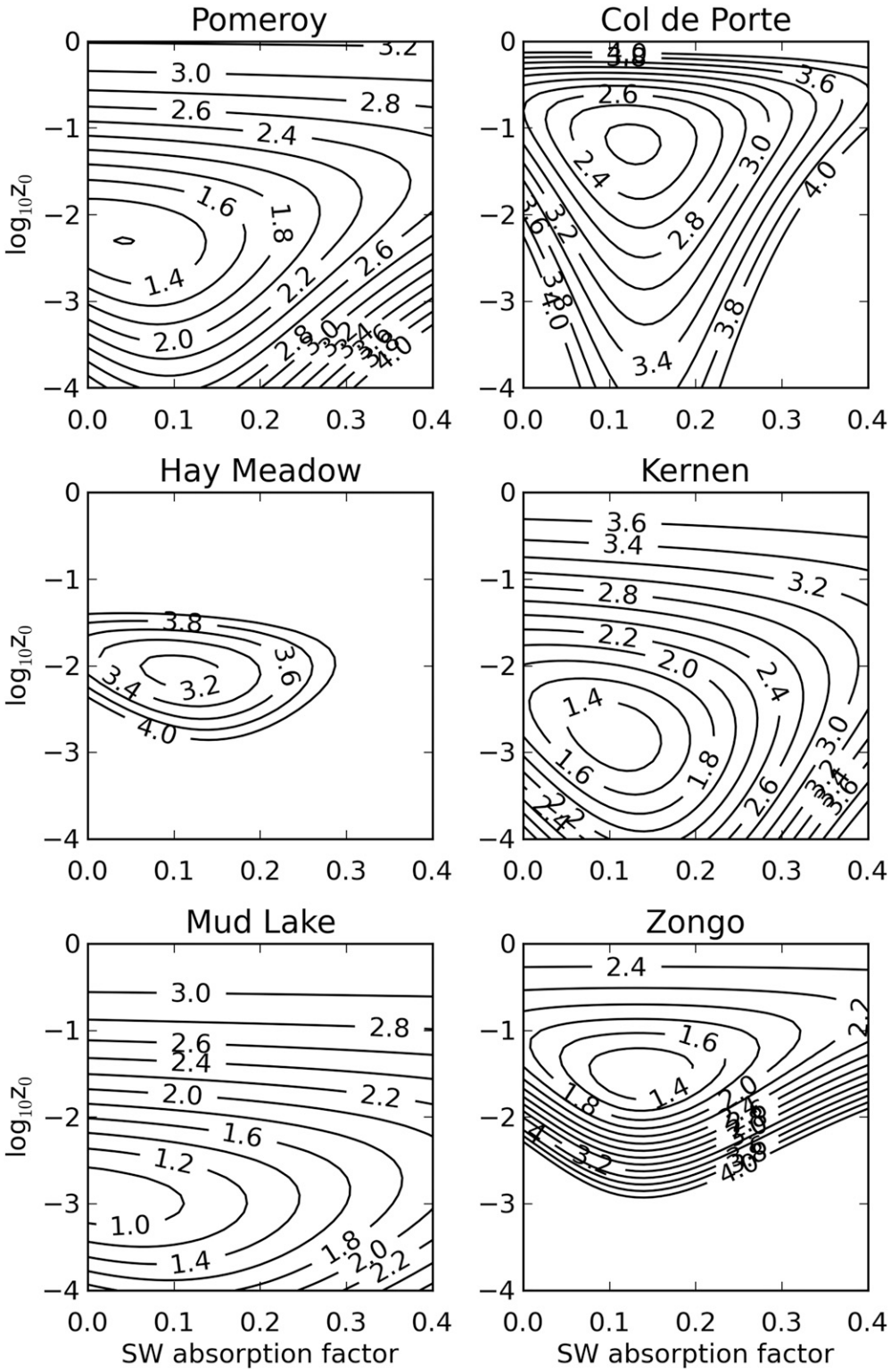

FIG. 5. Sensitivity of model RMSE (contour interval 0.2°C) to variations in shortwave radiation absorption and aerodynamic roughness parameters.

TABLE 2. Parameters, biases, and RMSEs for optimized snow surface temperature simulations.

	Shortwave absorption	Roughness (m)	Bias (K)	RMSE (K)
Pomeroy	0.05	0.005	0.26	1.20
Col de Porte	0.13	0.063	0.33	2.15
Hay Meadow	0.10	0.008	−0.04	3.13
Kernen	0.10	0.002	0.31	1.27
Mud Lake	0.00	0.001	0.17	0.86
Zongo	0.13	0.032	−0.02	1.22

inversions at night and excellent wind exposure on a high mountain. Overall, the range of f_v from 0.95 to 0.25 shows that both radiation and ventilation are important in controlling the SST and should be included in an SST model. Note that wind speeds were limited to a minimum value of 0.1 to avoid anemometer stalling. This amounts to an implicit windless exchange coefficient for these model tests and keeps the ventilation factor from reaching very small values.

To evaluate potential model performance with global parameters and the necessity of using shortwave radiation to drive the RPM, the model was run with 10% and 0% shortwave radiation absorption for smooth (0.003 m) and rough (0.03 m) aerodynamic roughness lengths for the complete dataset at all sites. The results are plotted as observed versus modeled data in Fig. 8, and the statistics for these simulations are listed in Table 3. The best global parameter simulations based on RMSE were for Mud Lake, Kernen Farm, Pomeroy Acreage, and Zongo Glacier—all sites with long open fetch, good wind exposure, and RMSEs <1.3 K. The best simulations based on bias were Pomeroy Acreage, Col de Porte, and Zongo Glacier. The poorest simulations based on RMSE and/or bias were for Hay Meadow and Col de Porte, which had forests nearby and RMSEs ranging from 2.3 to 3.5 K for the best set of global parameters. The only site with notably larger errors than the others is Hay Meadow. This site has an extremely gusty turbulent regime (Helgason

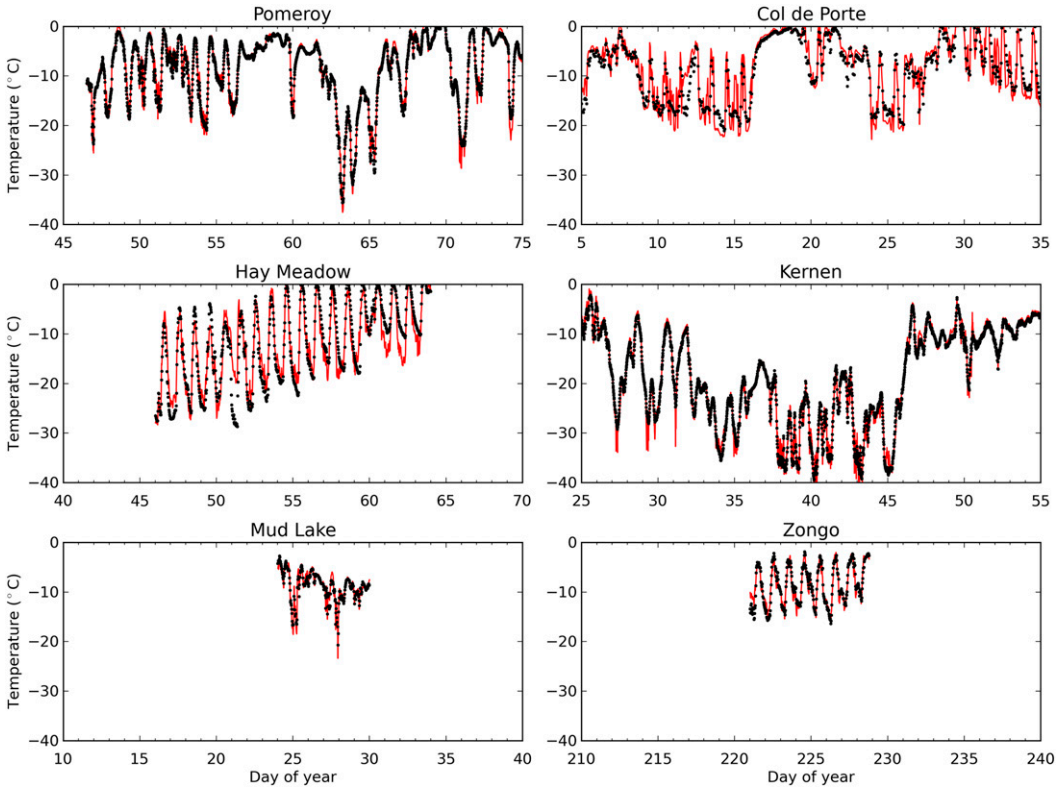

FIG. 6. SST measured (black dots) and modeled (red lines) with RPM at the six sites using optimized parameters from Table 2.

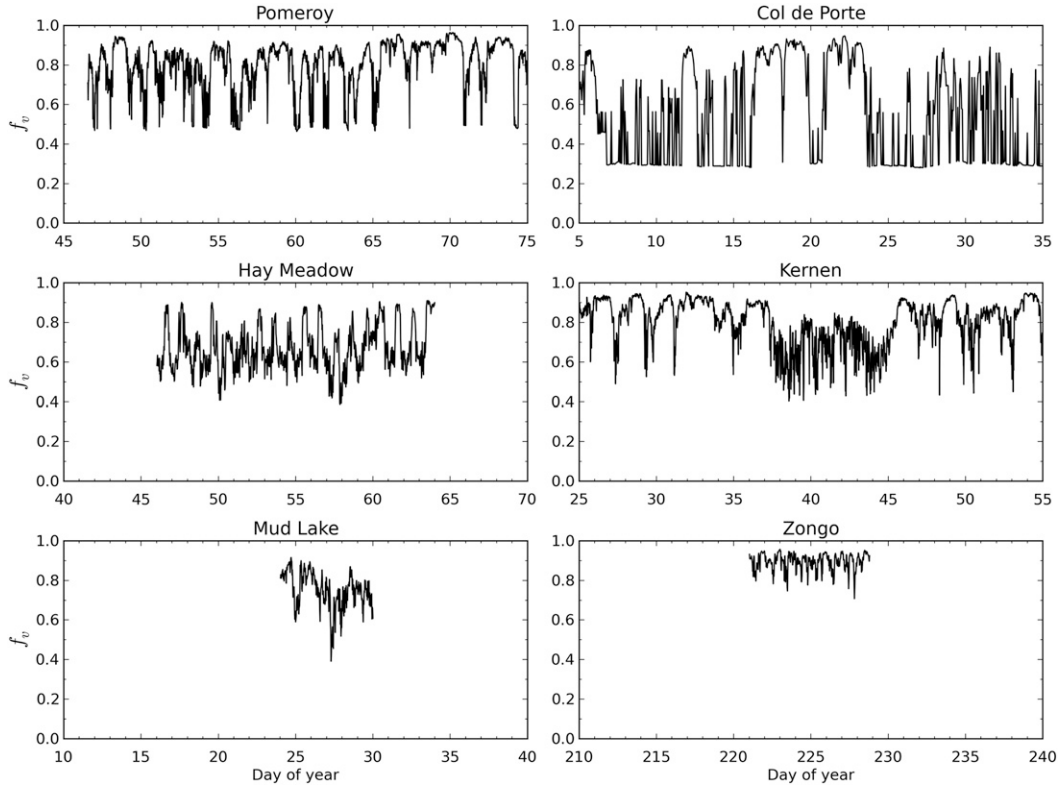

FIG. 7. Ventilation factor (i.e., f_v) at the six sites as calculated using the RPM.

and Pomeroy 2005) and sometimes had exposed grass above the snow. The gustiness of the site might have degraded the aerodynamic calculations, and the exposed grass may have affected surface temperature measurements. The parameter combination of smooth with 10% shortwave absorption provided the best simulations (RMSE) for the relatively level prairie and Hay Meadow mountain valley bottom sites while the rough and 10% shortwave absorption combination was optimal for the complex terrain sites of Col de Porte and Zongo Glacier. For the Mud Lake simulations (frozen lake snowpack, very clean snow, and low insolation period in midwinter), the optimal parameters were for zero shortwave absorption and a smooth aerodynamic roughness reflecting its extremely smooth and high albedo condition. There was no benefit to using shortwave radiation data to run the model for Mud Lake and little benefit at the prairie and mountain valley sites in Canada, as small differences in bias and RMSE show; however, RMSEs increased appreciably by from 0.85 to 1.66 K when radiation absorption was not included at the tropical and temperate mountain sites in Bolivia and France, where both high insolation and contamination of snow are more probable. It is clear that there is no one global parameter set, but that site information can be used to choose parameters from the set shown in boldface in Table 3 and demonstrated in Fig. 8. High-latitude sites where snowpacks are normally clean with relatively little dust deposition do not require consideration of shortwave absorption, while lower-latitude sites do. Sites on frozen lakes, in open valley bottoms, and on prairies are best served with a small aerodynamic roughness length, while those on glaciers and near forests and complex terrain should use a larger length. It is likely that a dynamical model of shortwave absorption would provide improved values for the absorption parameter and its seasonal evolution, but at the expense of a substantial increase in RPM complexity.

Any new model needs a test of its transferability to datasets not involved in its optimization or selection of global parameters. To test the RPM, the full 18-yr dataset from Col de Porte was used with the global parameter set for a rough aerodynamic surface with 10% shortwave absorption (Table 3), and results are shown in Fig. 9. The RMSE of 2.56 K and bias of −0.81 K are similar to the January 2006 data shown in Table 3 for the same global parameter set, suggesting model predictive stability despite climate variability and changes in site conditions and instrumentation over 18 years.

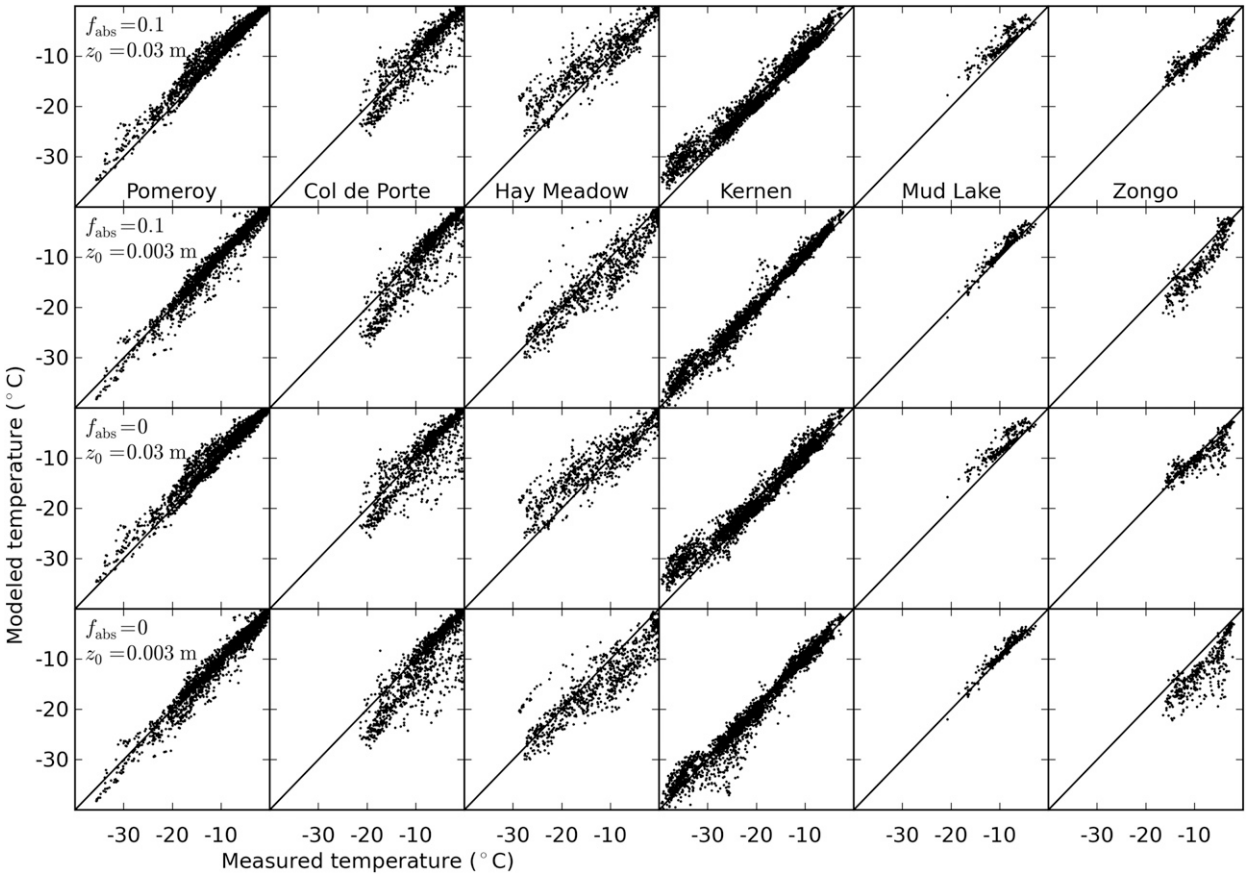

FIG. 8. Scatterplot of measured and RPM-simulated SST for the six sites with four sets of global parameters (0% or 10% SW absorption, 0.03 or 0.003 m roughness length).

Methods to estimate the SST that use the air temperature, dewpoint temperature, or ice bulb temperature (e.g., Raleigh et al. 2013) are attractive in that they only require information on atmospheric temperature and humidity and so have a requirement for fewer driving variables and parameters than the RPM. Unfortunately, these methods lack a physical basis to predict SST and so may not be able to accurately estimate it. To evaluate how well these methods could predict the SST over this dataset, their outputs were compared to observations and the results shown in Table 4. The RPM more accurately estimated SST than any of these approaches, with RMSE improvements ranging from 1.15 to 6.33 K. The more accurate of the simple methods were the ice bulb and dewpoint approaches with RMS difference with RPM of only 2.53 and 2.67 K, respectively. Errors from assuming the SST was equal to the air temperature were large, and the

TABLE 3. RMSEs (K) and bias (K) for simulations with global parameters (0% or 10% SW absorption, 0.03 m or 0.003 m roughness length). Smallest RMSEs and bias are in boldface. The global parameter sets selected are italicized.

	0% SW absorption				10% SW absorption			
	Smooth		Rough		Smooth		Rough	
	RMSE	Bias	RMSE	Bias	RMSE	Bias	RMSE	Bias
Pomeroy	1.33	**−0.22**	1.68	1.01	***1.30***	*0.24*	1.78	1.22
Col de Porte	4.22	−2.18	3.32	−0.99	2.94	−1.26	***2.31***	***−0.29***
Hay Meadow	4.33	−2.41	3.77	**1.33**	***3.52***	*−1.35*	3.73	1.87
Kernen	1.65	**0.16**	2.26	1.34	***1.33***	*0.59*	2.35	1.60
Mud Lake	***1.05***	***0.65***	2.18	1.75	1.18	0.81	2.23	1.82
Zongo	4.74	−3.86	2.14	−0.89	3.08	−2.43	***1.29***	***−0.22***

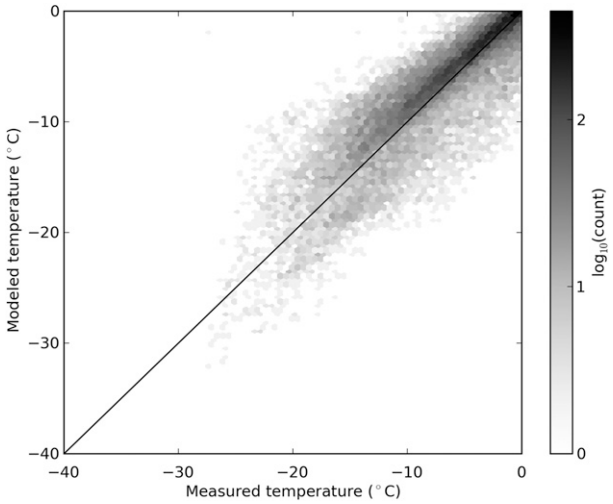

FIG. 9. Scatterplot using tonal density to show the number of points in small hexagons representing measured and modeled SST for Col de Porte over 18 years using the shortwave absorption factor of 0.1 and aerodynamic roughness height of 0.03 m.

RPM improved these simulations by an RMSE change of 4.19 K.

6. Conclusions

The SST is the critically important upper boundary condition for the snowpack and lower boundary condition for the atmosphere and so of great interest to snow scientists, hydrologists, and atmospheric scientists. Various methods have been used in snow, land surface, and hydrological models to estimate SST, and they principally include air temperature, force–restore, heat conduction, dewpoint, ice bulb, and coupled energy and mass balance calculations. The physically based coupled energy and mass balance methods require a greater number of driving variables and parameters and so have larger uncertainty due to these inputs than do the other methods, despite their physical correctness.

In an effort to reconcile model complexity, uncertainty, physical correctness, and simplicity to create a robust model for estimating SST, the primary driving processes that influence snow surface energetics were identified as aerodynamic (sensible and latent heat transfer) and radiative (thermal and near-infrared radiation). A new SST model, the radiative psychrometric model (RPM) was devised based on this understanding and written so that the radiative and aerodynamic factors controlling SST could be clearly identified. The RPM was tested against careful SST measurements at six sites in North America, South America, and Europe that span prairie, mountain, frozen lake, and glacier surfaces with various wind exposures and fetch characteristics and was found to perform very well in estimating the SST with optimized parameters for shortwave radiation absorption and aerodynamic roughness length. Global parameters for shortwave absorption and roughness length were identified and applied based on a site classification. High-latitude sites with clean snow remote from sources of dust and pollution do not need to consider shortwave absorption in RPM, while lower- and midlatitude sites that are proximal to particulate sources do. Sites on frozen lakes, in open valley bottoms, and on prairies are best served with a small aerodynamic roughness length, while those on glaciers and near forests and complex terrain should use a larger length. A test of the RPM with site-selected global parameters for a longer time span at Col de Porte showed good temporal transferability. A comparison of the RPM with recently proposed SST estimation methods shows that the RPM provides superior predictions of SST when compared to air temperature, dewpoint, or ice bulb calculation approaches.

TABLE 4. RMSEs (K) for approximating snow surface temperature by air temperature T_a, dewpoint temperature T_d, or wet bulb temperature T_w and the increase in RMSE (in parentheses) compared with those for the selected global parameters for IPM (selected set is italicized in Table 3).

	T_a	T_d	T_w
Pomeroy	3.87 (2.57)	3.00 (1.7)	3.27 (1.97)
Col de Porte	6.91 (4.6)	4.57 (2.26)	5.63 (3.32)
Hay Meadow	9.85 (6.33)	7.23 (3.71)	7.61 (4.09)
Kernen	3.96 (2.63)	3.52 (2.19)	3.82 (2.49)
Mud Lake	4.72 (3.67)	2.20 (1.15)	3.10 (2.05)
Zongo	6.63 (5.34)	6.28 (4.99)	2.56 (1.27)

Acknowledgments. The authors would like to acknowledge funding from NSERC, NERC, CFI, CFCAS, Canada Research Chairs, Global Institute for Water Security, Alberta Agriculture and Forestry, and IRD France. The assistance of many students and staff of the Centre for Hydrology over the years was essential to high quality data collection. Data provided by IRD France from Dr. J.E. Sicart and Météo-France from Dr. S. Morin is gratefully acknowledged.

REFERENCES

Andreas, E. L, 1986: A new method of measuring the snow-surface temperature. *Cold Reg. Sci. Technol.*, **12**, 139–156, doi:10.1016/0165-232X(86)90029-7.

Armstrong, R. L., and E. Brun, Eds., 2008: *Snow and Climate: Physical Processes, Surface Energy Exchange and Modeling.* Cambridge University Press, 222 pp.

Bartelt, P., and M. Lehning, 2002: A physical SNOWPACK model for the Swiss avalanche warning. Part I: Numerical model. *Cold Reg. Sci. Technol.*, **35**, 123–145, doi:10.1016/S0165-232X(02)00074-5.

Best, M. J., and Coauthors, 2011: The Joint UK Land Environment Simulator (JULES), model description. Part 1: Energy and water fluxes. *Geosci. Model Dev.*, **4**, 677–699, doi:10.5194/gmd-4-677-2011.

Brun, E., E. Martin, V. Simon, C. Gendre, and C. Coleau, 1989: An energy and mass balance model of snow cover suitable for operational avalanche forecasting. *J. Glaciol.*, **35**, 333–342.

——, P. David, M. Sudul, and G. Brunot, 1992: A numerical model to simulate snow-cover stratigraphy for operational avalanche forecasting. *J. Glaciol.*, **38**, 13–22.

Buck, A. L., 1981: New equations for computing vapor pressure and enhancement factor. *J. Appl. Meteor.*, **20**, 1527–1532, doi:10.1175/1520-0450(1981)020<1527:NEFCVP>2.0.CO;2.

Dang, C., R. E. Brandt, and S. G. Warren, 2015: Parameterizations for narrowband and broadband albedo of pure snow and snow containing mineral dust and black carbon. *J. Geophys. Res. Atmos.*, **120**, 5446–5468, doi:10.1002/2014JD022646.

Douville, H., J.-F. Royer, and J.-F. Mahfouf, 1995: A new snow parameterization for the Météo-France climate model. *Climate Dyn.*, **12**, 21–35, doi:10.1007/BF00208760.

Dozier, J., and S. G. Warren, 1982: Effect of viewing angle on the infrared brightness temperature of snow. *Water Resour. Res.*, **18**, 1424–1434, doi:10.1029/WR018i005p01424.

Ellis, C. R., J. W. Pomeroy, T. Brown, and J. MacDonald, 2010: Simulation of snow accumulation and melt in needleleaf forest environments. *Hydrol. Earth Syst. Sci.*, **14**, 925–940, doi:10.5194/hess-14-925-2010.

Essery, R., S. Morin, Y. Lejeune, and C. B. Ménard, 2013: A comparison of 1701 snow models using observations from an alpine site. *Adv. Water Resour.*, **55**, 131–148, doi:10.1016/j.advwatres.2012.07.013.

Fierz, C., P. Riber, E. E. Adams, A. R. Curran, P. M. B. Föhn, M. Lehning, and C. Plüss, 2003: Evaluation of snow-surface energy balance models in alpine terrain. *J. Hydrol.*, **282**, 76–94, doi:10.1016/S0022-1694(03)00255-5.

Gray, D. M., and P. G. Landine, 1988: An energy-budget snowmelt model for the Canadian Prairies. *Can. J. Earth Sci.*, **25**, 1292–1303, doi:10.1139/e88-124.

Hachikubo, A., and E. Akitaya, 1997: Effect of wind on surface hoar growth on snow. *J. Geophys. Res.*, **102**, 4367–4373, doi:10.1029/96JD03456.

Helgason, W. D., and J. W. Pomeroy, 2005: Uncertainties in estimating turbulent fluxes to melting snow in a mountain clearing. *Proc. 62nd Eastern Snow Conf.*, Waterloo, ON, Canada, Eastern Snow Conference, 129–142. [Available online at http://www.easternsnow.org/proceedings/2005/helgason.pdf.]

——, and ——, 2012a: Characteristics of the near-surface boundary layer within a mountain valley during winter. *J. Appl. Meteor. Climatol.*, **51**, 583–597, doi:10.1175/JAMC-D-11-058.1.

——, and ——, 2012b: Problems closing the energy balance over a homogeneous snow cover during midwinter. *J. Hydrometeor.*, **13**, 557–572, doi:10.1175/JHM-D-11-0135.1.

Hori, M., and Coauthors, 2006: In-situ measured spectral directional emissivity of snow and ice in the 8–14 μm atmospheric window. *Remote Sens. Environ.*, **100**, 486–502, doi:10.1016/j.rse.2005.11.001.

Jordan, R. E., 1991: A one-dimensional temperature model for a snow cover: Technical documentation for SNTERERM.89. Special Rep. 91-16, Cold Region Research and Engineers Laboratory, U.S. Army Corps of Engineers, Hanover, NH, 61 pp.

King, J., J. W. Pomeroy, D. M. Gray, C. Fierz, P. Föhn, and Coauthors, 2008: Snow–atmosphere energy and mass balance. *Snow and Climate: Physical Processes, Surface Energy Exchange and Modeling*, R. L. Armstrong and E. Brun, Eds., Cambridge University Press, 70–124.

Koh, G., and R. Jordan, 1995: Sub-surface melting in a seasonal snow cover. *J. Glaciol.*, **41**, 474–482.

Kondo, J., and T. Yamazaki, 1990: A prediction model for snowmelt, snow surface temperature and freezing depth using a heat balance method. *J. Appl. Meteor.*, **29**, 375–384, doi:10.1175/1520-0450(1990)029<0375:APMFSS>2.0.CO;2.

Lehning, M., P. Bartelt, R. L. Brown, and C. Fierz, 2002: A physical SNOWPACK model for the Swiss avalanche warning: Part III: Meteorological forcing, thin layer formation and evaluation. *Cold Reg. Sci. Technol.*, **35**, 169–184, doi:10.1016/S0165-232X(02)00072-1.

Luce, C. H., and D. G. Tarboton, 2010: Evaluation of alternative formulae for calculation of surface temperature in snowmelt models using frequency analysis of temperature observations. *Hydrol. Earth Syst. Sci.*, **14**, 535–543, doi:10.5194/hess-14-535-2010.

Marks, D., and J. Dozier, 1992: Climate and energy exchange at the snow surface in the Alpine region of the Sierra Nevada: 2. Snow cover energy balance. *Water Resour. Res.*, **28**, 3043–3054, doi:10.1029/92WR01483.

——, J. Domingo, D. Susong, T. Link, and D. Garen, 1999: A spatially distributed energy balance snowmelt model for application in mountain basins. *Hydrol. Processes*, **13**, 1935–1959, doi:10.1002/(SICI)1099-1085(199909)13:12/13<1935::AID-HYP868>3.0.CO;2-C.

——, A. Winstral, G. Flerchinger, M. Reba, J. Pomeroy, T. Link, and K. Elder, 2008: Comparing simulated and measured sensible and latent heat fluxes over snow under a pine canopy to improve an energy balance snowmelt model. *J. Hydrometeor.*, **9**, 1506–1522, doi:10.1175/2008JHM874.1.

Marsh, P., and J. W. Pomeroy, 1996: Meltwater fluxes at an arctic forest–tundra site. *Hydrol. Processes*, **10**, 1383–1400, doi:10.1002/(SICI)1099-1085(199610)10:10<1383::AID-HYP468>3.0.CO;2-W.

Martin, E., and Y. Lejeune, 1998: Turbulent fluxes above the snow surface. *Ann. Glaciol.*, **26**, 179–183.

Morin, S., Y. Lejeune, B. Lesaffre, J.-M. Panel, D. Poncet, P. David, and M. Sudul, 2012: A 18-yr long (1993–2011) snow and meteorological dataset from a mid-altitude mountain site (Col de Porte, France, 1325 m alt.) for driving and evaluating snowpack models. *Earth Syst. Sci. Data*, **4**, 13–21, doi:10.5194/essd-4-13-2012.

Oleson, K. W., and Coauthors, 2008: Improvements to the Community Land Model and their impact on the hydrological cycle. *J. Geophys. Res.*, **113**, G01021, doi:10.1029/2007JG000563.

Pomeroy, J. W., and E. Brun, 2001: Physical properties of snow. *Snow Ecology*, H. G. Jones et al., Eds., Cambridge University Press, 45–126.

——, D. M. Gray, K. R. Shook, B. Toth, R. L. H. Essery, A. Pietroniro, and N. Hedstrom, 1998: An evaluation of snow accumulation and ablation processes for land surface modelling. *Hydrol. Processes*, **12**, 2339–2367, doi:10.1002/(SICI)1099-1085(199812)12:15<2339::AID-HYP800>3.0.CO;2-L.

Raj Singh, P., and T. Yew Gan, 2005: Modelling snowpack surface temperature in the Canadian Prairies using simplified heat flow models. *Hydrol. Processes*, **19**, 3481–3500, doi:10.1002/hyp.5839.

Raleigh, M. S., C. C. Landry, M. Hayashi, W. L. Quinton, and J. D. Lundquist, 2013: Approximating snow surface temperature

from standard temperature and humidity data: New possibilities for snow model and remote sensing evaluation. *Water Resour. Res.*, **49**, 8053–8069, doi:10.1002/2013WR013958.

Rutter, N., and Coauthors, 2009: Evaluation of forest snow processes models (SnowMIP2). *J. Geophys. Res.*, **114**, D06111, doi:10.1029/2008JD011063.

Schirmer, M., and B. Jamieson, 2014: Limitations of using a thermal imager for snow pit temperatures. *Cryosphere*, **8**, 387–394, doi:10.5194/tc-8-387-2014.

Sicart, J. E., P. Wagnon, and P. Ribstein, 2005: Atmospheric controls of the heat balance of Zongo Glacier (16°S, Bolivia). *J. Geophys. Res.*, **110**, D12106, doi:10.1029/2004JD005732.

Slater, A. G., and Coauthors, 2001: The representation of snow in land surface schemes: Results from PILPS 2(d). *J. Hydrometeor.*, **2**, 7–25, doi:10.1175/1525-7541(2001)002<0007:TROSIL>2.0.CO;2.

Stössel, F., M. Guala, C. Fierz, C. Manes, and M. Lehning, 2010: Micrometeorological and morphological observations of surface hoar dynamics on a mountain snow cover. *Water Resour. Res.*, **46**, W04511, doi:10.1029/2009WR008198.

Tarboton, D. G., and C. H. Luce, 1996: Utah Energy Balance Snow Accumulation and Melt Model (UEB): Computer model technical description users guide. Utah Water Research Laboratory/USDA Forest Service Intermountain Research Station, 64 pp. [Available online at http://www.fs.fed.us/rm/boise/publications/watershed/rmrs_1996_tarbotond001.pdf.]

Verseghy, D. L., 1991: Class—A Canadian land surface scheme for GCMS. I. Soil model. *Int. J. Climatol.*, **11**, 111–133, doi:10.1002/joc.3370110202.

——, N. A. McFarlane, and M. Lazare, 1993: Class—A Canadian land surface scheme for GCMS, II. Vegetation model and coupled runs. *Int. J. Climatol.*, **13**, 347–370, doi:10.1002/joc.3370130402.

Vionnet, V., E. Brun, S. Morin, A. Boone, S. Faroux, P. Le Moigne, E. Martin, and J.-M. Willemet, 2012: The detailed snowpack scheme Crocus and its implementation in SURFEX v7.2. *Geosci. Model Dev.*, **5**, 773–791, doi:10.5194/gmd-5-773-2012.

Warren, S. G., and W. J. Wiscombe, 1980: A model for the spectral albedo of snow. II: Snow containing atmospheric aerosols. *J. Atmos. Sci.*, **37**, 2734–2745, doi:10.1175/1520-0469(1980)037<2734:AMFTSA>2.0.CO;2.

Wiscombe, W. J., and S. G. Warren, 1980: A model for the spectral albedo of snow. I: Pure snow. *J. Atmos. Sci.*, **37**, 2712–2733, doi:10.1175/1520-0469(1980)037<2712:AMFTSA>2.0.CO;2.